Stochastic Modeling of Flow-Structure Interactions Using Generalized Polynomial Chaos

Dongbin Xiu

Didier Lucor

C.-H. Su

George Em Karniadakis[1]

Division of Applied Mathematics,
Brown University,
Providence, RI 02912

We present a generalized polynomial chaos algorithm to model the input uncertainty and its propagation in flow-structure interactions. The stochastic input is represented spectrally by employing orthogonal polynomial functionals from the Askey scheme as the trial basis in the random space. A standard Galerkin projection is applied in the random dimension to obtain the equations in the weak form. The resulting system of deterministic equations is then solved with standard methods to obtain the solution for each random mode. This approach is a generalization of the original polynomial chaos expansion, which was first introduced by N. Wiener (1938) and employs the Hermite polynomials (a subset of the Askey scheme) as the basis in random space. The algorithm is first applied to second-order oscillators to demonstrate convergence, and subsequently is coupled to incompressible Navier-Stokes equations. Error bars are obtained, similar to laboratory experiments, for the pressure distribution on the surface of a cylinder subject to vortex-induced vibrations. [DOI: 10.1115/1.1436089]

1 Introduction

In the last decade there has been substantial progress in simulations of flow-structure interactions involving the full Navier-Stokes equations, e.g. [1,2]. While such simulations are useful in complementing experimental studies in the low Reynolds number range, they are based on *ideal* boundary conditions and *precisely* defined properties of the structure. In practice, such flow conditions and properties can only be defined approximately. As an example, the internal structural damping for the structure is typically taken as 1–3 percent of the critical damping since it cannot be quantified by direct measurements. It is, therefore, of great interest to formally model such uncertainty of stochastic inputs, and to formulate algorithms that reflect accurately the propagation of this uncertainty [3].

To this end, the Monte Carlo approach can be employed but it is computationally expensive and is only used as the last resort. The sensitivity method is a more economical approach, based on the moments of samples, but it is less robust and depends strongly on the modeling assumptions [4]. One popular technique is the perturbation method where all the stochastic quantities are expanded around their mean via Taylor series. This approach, however, is limited to small perturbations and does not readily provide information on high-order statistics of the response. The resulting system of equations becomes extremely complicated beyond second-order expansion. Another approach is based on expanding the inverse of the stochastic operator in a Neumann series, but this too is limited to small fluctuations, and even combinations with the Monte Carlo method seem to result in computationally prohibitive algorithms for complex systems [5].

A more effective approach pioneered by Ghanem and Spanos [6] in the context of finite elements for solid mechanics is based on a spectral representation of the uncertainty. This allows high-order representation, not just first-order as in most perturbation-based methods, at high computational efficiency. It is based on the original theory of Wiener (1938) on homogeneous chaos [7,8]. This approach was employed in turbulence in the 1960s [9–11]. However, it was realized that the chaos expansion converges slowly for turbulent fields [12–14], so the polynomial chaos approach did not receive much attention for a long time.

In more recent work [15,16] the polynomial chaos concept was extended to represent many different distribution functions. This generalized polynomial chaos approach, also referred as the Askey-chaos, employs the orthogonal polynomials from the Askey scheme [17] as the trial basis in the random space. The original polynomial chaos can be considered as a subset of the generalized polynomial chaos, as it employs Hermite polynomials, a subset of the Askey scheme, as the trial basis. In [15], the framework of Askey-chaos was proposed and convergence properties of different random bases were examined. In [16] the Askey-chaos was applied to model uncertainty in incompressible Navier-Stokes equations. Various tests were conducted to demonstrate the convergence of the chaos expansion in prototype flows.

For flow-structure interactions the interest on stochastic modeling so far has primarily been on the dynamics of lumped systems, i.e., single- or two-degree-of-freedom second-order oscillators [18,19]. The effect of the flow has been modeled via an interaction (source) term as either white noise or as a Gaussian distribution if the loading is caused by wind [20–23]. However, non-Gaussian distribution behavior for the response has been documented with *the excess index* well above or below zero (sharp or flat intermittency) [18]. For example, even for a velocity field following a Gaussian distribution, which is a reasonable assumption for maritime winds [21], the corresponding force given by the Morison formula

$$F_V(t) = \tfrac{1}{2}\rho D C_d V(t)|V(t)|$$

does not follow a Gaussian distribution. This is because the above formula defines a nonlinear (memoryless) transformation [20], and its first-density function is given by

$$f_1(v) = \frac{1}{2\sigma_V \sqrt{2\pi|v|}} \exp\left[-\frac{1}{2}\left(\frac{sign(v)\sqrt{|v|} - m_V}{\sigma_V} \right)^2 \right],$$

where m_V and σ_V are the mean value and standard deviation of the the Gaussian distribution for the velocity $V(t)$.

In this paper we apply the chaos expansions to coupled Navier-Stokes/structure equations. We first demonstrate the convergence of chaos expansions by solving a second-order ordinary differential equation. We then present the stochastic modeling of the fully coupled flow-structure interaction problem for vortex-induced vi-

brations in flow past a cylinder. The algorithms developed here are general and can be applied to any type of distributions although our applications are concentrated on Gaussian type random inputs.

In the next section we review the theory of the generalized polynomial chaos. In Section 3 we apply it to second-order oscillators, and in Section 4 we present its application to Navier-Stokes equations. In Section 5 we present the computational results of stochastic flow-structure interactions, and we conclude with a brief discussion in Section 6.

2 The Generalized Polynomial Chaos

In this section we introduce the generalized polynomial chaos expansion along with the Karhunen-Loeve (KL) expansion, another classical technique for representing random processes. The KL expansion can be used in some cases to represent efficiently the known stochastic fields, i.e., the stochastic inputs.

2.1 The Askey Scheme. The Askey scheme, which is represented as a tree structure in Fig. 1 (following [24]), classifies the hypergeometric orthogonal polynomials and indicates the limit relations between them. The "tree" starts with the Wilson polynomials and the Racah polynomials on the top. The Wilson polynomials are continuous while the Racah polynomials are discrete. The lines connecting different polynomials denote the limit transition relationships between them; this implies that the polynomials at the lower end of the lines can be obtained by taking the limit of one of the parameters from their counterparts on the upper end. For example, the limit relation between Jacobi polynomials $P_n^{(\alpha,\beta)}(x)$ and Hermite polynomials $H_n(x)$ is

$$\lim_{\alpha \to \infty} \alpha^{-1/2n} P_n^{(\alpha,\alpha)}\left(\frac{x}{\sqrt{\alpha}}\right) = \frac{H_n(x)}{2^n n!},$$

and between Meixner polynomials $M_n(x;\beta,c)$ and Charlier polynomials $C_n(x;a)$ is

$$\lim_{\beta \to \infty} M_n\left(x;\beta,\frac{a}{a+\beta}\right) = C_n(x;a).$$

For a detailed account of definitions and properties of hypergeometric polynomials, see [17]; for the limit relations of Askey scheme, see [25] and [24].

The orthogonal polynomials associated with the generalized polynomial chaos, include: Hermite, Laguerre, Jacobi, Charlier, Meixner, Krawtchouk, and Hahn polynomials.
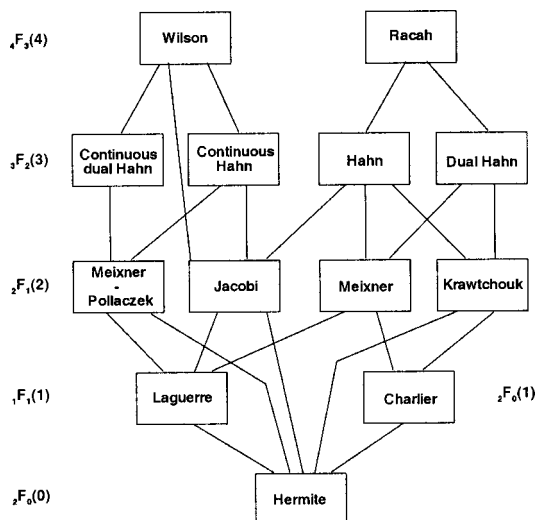

Fig. 1 The Askey scheme of orthogonal polynomials

Table 1 Correspondence of the type polynomials and random variables for different Askey-chaos ($N \geq 0$ is a finite integer).

	Random variables ξ	Orthogonal polynomials $\{I_n\}$	Support
Continuous	Gaussian	Hermite	$(-\infty,\infty)$
	Gamma	Laguerre	$[0,\infty)$
	Beta	Jacobi	$[a,b]$
	Uniform	Legendre	$[a,b]$
Discrete	Poisson	Charlier	$\{0,1,2,\dots\}$
	Binomial	Krawtchouk	$\{0,1,\dots,N\}$
	Negative Binomial	Meixner	$\{0,1,2,\dots\}$
	Hypergeometric	Hahn	$\{0,1,\dots,N\}$

2.2 The Generalized Polynomial Chaos: Askey-Chaos. The original polynomial chaos [7,8] employs the Hermite polynomials in the random space as the trial basis to expand the stochastic processes. Cameron and Martin proved that such expansion converges to any second-order processes in the L_2 sense [26]. It can be seen from Fig. 1 that Hermite polynomial is a subset of the Askey scheme. The generalized polynomial chaos, or the Askey-Chaos, was proposed in [15,16] and employs more polynomials from the Askey scheme. Convergence to second-order stochastic processes can be readily obtained as a generalization of Cameron-Martin theorem [26].

A general second-order random process $X(\theta)$, viewed as a function of $\theta \in (0,1)$, i.e., the random event, can be represented in the form

$$X(\theta) = a_0 I_0 + \sum_{i_1=1}^{\infty} c_{i_1} I_1(\xi_{i_1}(\theta)) + \sum_{i_1=1}^{\infty} \sum_{i_2=1}^{i_1} c_{i_1 i_2} I_2(\xi_{i_1}(\theta),\xi_{i_2}(\theta))$$

$$+ \sum_{i_1=1}^{\infty} \sum_{i_2=1}^{i_1} \sum_{i_3=1}^{i_2} c_{i_1 i_2 i_3} I_3(\xi_{i_1}(\theta),\xi_{i_2}(\theta),\xi_{i_3}(\theta)) + \dots,$$

(1)

where $I_n(\xi_{i_1},\dots,\xi_{i_n})$ denotes the Askey-chaos of order n in terms of the multi-dimensional random variables $\xi = (\xi_{i_1},\dots,\xi_{i_n})$. In the original polynomial chaos, $\{I_n\}$ are *Hermite* polynomials and ξ are *Gaussian* random variables. In the Askey-chaos expansion, the polynomials I_n are not restricted to Hermite polynomials and ξ not Gaussian variables. The corresponding type of polynomials and their associated random variables are listed in Table 1.

For notational convenience, we rewrite Eq. (1) as

$$X(\theta) = \sum_{j=0}^{\infty} \hat{c}_j \Phi_j(\xi),$$

(2)

where there is a one-to-one correspondence between the functions $I_n(\xi_{i_1},\dots,\xi_{i_n})$ and $\Phi_j(\xi)$, and their coefficients $\hat{c}_j$ and $c_{i_1,\dots,i_r}$. Since each type of polynomials from the Askey scheme form a complete basis in the Hilbert space determined by their corresponding support, we can expect each type of Askey-chaos to converge to any L_2 functional in the L_2 sense in the corresponding Hilbert functional space as a generalized result of Cameron-Martin theorem ([26] and [27]). The orthogonality relation of the generalized polynomial chaos takes the form

$$\langle \Phi_i \Phi_j \rangle = \langle \Phi_i^2 \rangle \delta_{ij},$$

(3)

where δ_{ij} is the Kronecker delta and $\langle \cdot,\cdot \rangle$ denotes the ensemble average which is the inner product in the Hilbert space of the random variables ξ

$$\langle f(\xi)g(\xi) \rangle = \int f(\xi)g(\xi)W(\xi)d\xi,$$

(4)

or

$$\langle f(\boldsymbol{\xi})g(\boldsymbol{\xi})\rangle = \sum_{\xi} f(\boldsymbol{\xi})g(\boldsymbol{\xi})W(\boldsymbol{\xi}) \tag{5}$$

in the discrete case. Here $W(\boldsymbol{\xi})$ is the weighting function corresponding to the Askey polynomials chaos basis $\{\Phi_i\}$. Each type of orthogonal polynomials from the Askey-chaos has weighting functions of the same form as the probability function of its associated random variables $\boldsymbol{\xi}$, as shown in Table 1.

For example, as a subset of the Askey-chaos, the original polynomial chaos, also will be termed the Hermite-chaos, employs the Hermite polynomials defined as

$$I_n(\xi_{i_1}, \ldots, \xi_{i_n}) = e^{1/2\xi^T\xi}(-1)^n\frac{\partial^n}{\partial\xi_{i_1}\ldots\partial\xi_{i_n}}e^{-1/2\xi^T\xi}, \tag{6}$$

where $\boldsymbol{\xi} = (\xi_{i_1}, \ldots, \xi_{i_n})$ are multi-dimensional independent Gaussian random variables with zero mean and unit variance. The weight function in the orthogonality relation (4) is

$$W(\boldsymbol{\xi}) = \frac{1}{\sqrt{(2\pi)^n}}e^{-1/2\xi^T\xi}, \tag{7}$$

where n is the dimension of $\boldsymbol{\xi}$. It can seen that this is the same as the probability density function (PDF) of the n-dimensional Gaussian random variables. For example, the one-dimensional Hermite polynomials are:

$$\Psi_0 = 1, \quad \Psi_1 = \xi, \quad \Psi_2 = \xi^2 - 1, \quad \Psi_3 = \xi^3 - 3\xi, \ldots \tag{8}$$

2.3 The Karhunen-Loeve Expansion. The Karhunen-Loeve (KL) expansion [28] is another way of representing a random process. It is a spectral expansion based on the decomposition of the covariance function of the process. Let us denote the process by $h(\mathbf{x}, \theta)$ and its covariance function by $R_{hh}(\mathbf{x}, \mathbf{y})$, where $\mathbf{x}$ and $\mathbf{y}$ are the spatial or temporal coordinates. By definition, the covariance function is real, symmetric, and positive definite. All eigenfunctions are mutually orthogonal and form a complete set spanning the function space to which $h(\mathbf{x}, \theta)$ belongs. The KL expansion then takes the following form:

$$h(\mathbf{x}, \theta) = \bar{h}(\mathbf{x}) + \sum_{i=1}^{\infty} \sqrt{\lambda_i}\phi_i(\mathbf{x})\xi_i(\theta), \tag{9}$$

where $\bar{h}(\mathbf{x})$ denotes the mean of the random process, and $\xi_i(\theta)$ forms a set of independent random variables. Also, $\phi_i(\mathbf{x})$ and λ_i are the eigenfunctions and eigenvalues of the covariance function, respectively, i.e.,

$$\int R_{hh}(\mathbf{x}, \mathbf{y})\phi_i(\mathbf{y})d\mathbf{y} = \lambda_i\phi_i(\mathbf{x}). \tag{10}$$

Among many possible decompositions of a random process, the KL expansion is optimal in the sense that the mean-square error of the finite term representation of the process is minimized. Its use, however, is limited as the covariance function of the solution process is often not known *a priori*. Nevertheless, the KL expansion provides an effective means of representing the input random processes when the covariance structure is known.

3 Second-order Random Oscillator

3.1 Governing Equations. We consider the second-order linear ordinary differential equation (ODE) system with both external and parametric random excitations.

$$\frac{dx}{dt} = y, $$

$$\frac{dy}{dt} + c(\theta)y + k(\theta)x = f(t, \theta), \tag{11}$$

where the parameters and forcing are functions of random event θ. We assume

$$c = \bar{c} + \sigma_c\xi_1, \quad k = \bar{k} + \sigma_k\xi_2, $$

$$f(t) = F\cos(\omega t) = (\bar{f} + \sigma_f\xi_3)\cos(\omega t), \tag{12}$$

where $(\bar{c}, \sigma_c)$, $(\bar{k}, \sigma_k)$ and $(\bar{f}, \sigma_f)$ are the mean and standard deviation of c, k and F, respectively. The random variables ξ_1, ξ_2, and ξ_3 are assumed to be independent standard *Gaussian* random variables.

3.2 Chaos Expansions. By applying the generalized polynomial chaos expansion, we expand the solutions as

$$x(t) = \sum_{i=0}^{P} x_i(t)\Phi_i(\boldsymbol{\xi}), \quad y(t) = \sum_{i=0}^{P} y_i(t)\Phi_i(\boldsymbol{\xi}), \tag{13}$$

where we have replaced the infinite summation of $\boldsymbol{\xi}$ in infinite dimensions in Eq. (2) by a truncated finite-term summation of $\boldsymbol{\xi}$ in finite dimensional space. In this case, $\boldsymbol{\xi} = (\xi_1, \xi_2, \xi_3)$ is a three-dimensional *Gaussian* random vector according to the random inputs. This results in a three-dimensional *Hermite*-chaos expansion. The most important aspect of the above expansion is that the random processes have been decomposed into a set of deterministic functions in the spatial-temporal variables multiplied by the random basis polynomials which are independent of these variables:

$$\sum_{k=0}^{P}\frac{dx_k}{dt}\Phi_k = \sum_{k=0}^{P} y_k\Phi_k, $$

$$\sum_{k=0}^{P}\frac{dy_k}{dt}\Phi_k + \sum_{i=0}^{P}\sum_{j=0}^{P} c_iy_j\Phi_i\Phi_j$$

$$+ \sum_{i=0}^{P}\sum_{j=0}^{P} k_ix_j\Phi_i\Phi_j = \sum_{k=0}^{P} f_k(t)\Phi_k, \tag{14}$$

where c_i, k_i, and f_i are the chaos expansion, similar to Eq. (13), of c, k, and f, respectively. A Galerkin projection of the above equation onto each polynomial basis $\{\Phi_i\}$ is then conducted in order to ensure the error is orthogonal to the functional space spanned by the finite-dimensional basis $\{\Phi_i\}$. By projecting with Φ_k for each $k = \{0, \ldots, P\}$ and employing the orthogonality relation (3), we obtain for each $k = 0, \ldots, P$,

$$\frac{dx_k}{dt} = y_k, $$

$$\frac{dy_k}{dt} + \frac{1}{\langle\Phi_k^2\rangle}\sum_{i=0}^{P}\sum_{j=0}^{P}(c_iy_j + k_ix_j)e_{ijk} = f_k(t), \tag{15}$$

where $e_{ijk} = \langle\Phi_i\Phi_j\Phi_k\rangle$. Together with $\langle\Phi_i^2\rangle$, the coefficients e_{ijk} can be evaluated analytically from the definition of Φ_i. Equation (15) is a set of $(P+1)$ coupled ODEs. The total number of equation is determined by the dimensionality of the chaos expansion (n), in this case ($n=3$), and the highest order (p) of the polynomials $\{\Phi\}$ [6]:

$$P = \sum_{s=1}^{p}\frac{1}{s!}\prod_{r=0}^{s-1}(n+r). \tag{16}$$

3.3 Numerical Results. The above set of equations can be integrated by any conventional method, e.g., Runge-Kutta. Here we employ the Newmark scheme which is second-order accurate in time. We define two error measures for the mean and variance of the solution
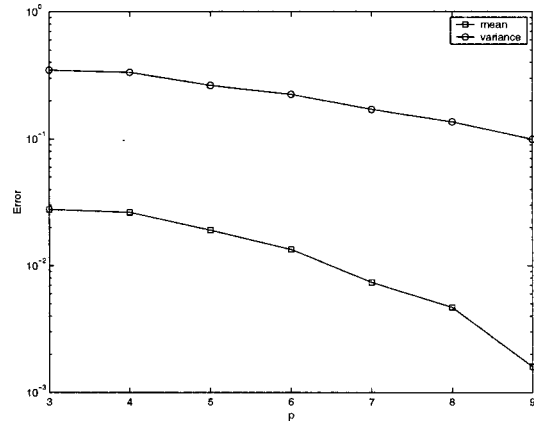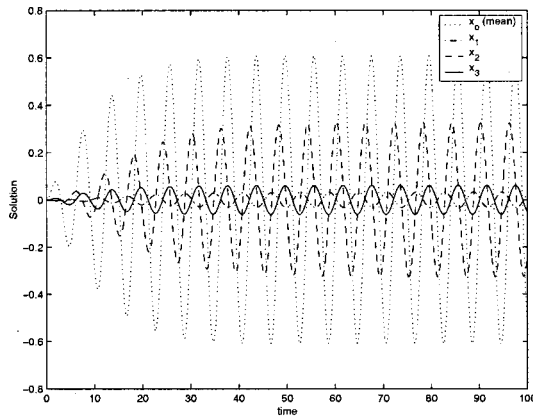
Fig. 2 Solution with Gaussian random inputs by Hermite-chaos. Left: solution of the dominant random modes, right: error convergence of the mean and the variance.

$$\varepsilon_{\mathrm{mean}}(T) = \left| \frac{\bar{x}(T) - \bar{x}_{\mathrm{exact}}(T)}{\bar{x}_{\mathrm{exact}}(T)} \right|, \quad \varepsilon_{\mathrm{var}}(T) = \left| \frac{\sigma^2(T) - \sigma^2_{\mathrm{exact}}(T)}{\sigma^2_{\mathrm{exact}}(T)} \right|,$$

(17)

where $\bar{x}(t) = E[x(t)]$ is the mean value of $x(t)$ and $\sigma^2(t) = E[(x(t) - \bar{x}(t))^2]$ is the variance. Integration is performed up to $T = 100$ (nondimensional time units) when the solution reaches an asymptotic periodic state. The computation parameters are set as: $(\bar{c}, \sigma_c) = (0.1, 0.01)$, $(\bar{k}, \sigma_k) = (1.05, 0.105)$ and $(\bar{f}, \sigma_f) = (0.1, 0.01)$, with frequency $\omega = 1.05$ and zero initial conditions. Here the standard deviations are set to be reasonably small to ensure the well-posedness of Eq. (11) in some stochastic sense. The exact stochastic solution is obtained from the exact deterministic solution and the known probability distribution functions of the random inputs. The exact mean and variance of the solution are obtained by integrating the solution over the support defined by the Gaussian distribution. These integrations are performed numerically using a Gauss-Hermite quadrature; a quadrature with 30 points provides high accuracy.

In Fig. 2 (left) we plot the development of the solution of the *mean* (zero mode) as well as the first three random modes, i.e., the modes contribution to a Gaussian distribution in this case. On the right figure we plot the error in the *mean* and the *variance*. We see from the semi-log plot that as the order of Hermite-chaos expansion increases, the error of mean and variance decreases exponentially fast. This is due to the fact that the chaos expansion is a spectral expansion in the random space. Similar exponential convergence rate has been demonstrated for first-order ODE for various Askey-chaos basis in [15]. It is worth noting that if the appropriate chaos basis, in this case the Hermite-chaos corresponding to the Gaussian inputs, is not chosen, the exponential convergence may not be maintained [15].

4 Incompressible Navier-Stokes Equations

In this section we present the solution procedure for solving the stochastic Navier-Stokes equations by generalized polynomial chaos expansion. The randomness in the solution can be introduced through boundary conditions, initial conditions, forcing, etc.

4.1 Governing Equations. We employ the incompressible Navier-Stokes equations

$$\nabla \cdot \mathbf{u} = 0,$$

(18)

$$\frac{\partial \mathbf{u}}{\partial t} + (\mathbf{u} \cdot \nabla) \mathbf{u} = -\nabla \Pi + \mathrm{Re}^{-1} \nabla^2 \mathbf{u},$$

(19)

where Π is the pressure and Re the Reynolds number. All flow quantities, i.e., velocity and pressure are considered as stochastic processes. A random dimension, denoted by the parameter θ, is introduced in addition to the spatial-temporal dimensions $(\mathbf{x}, t)$, thus

$$\mathbf{u} = \mathbf{u}(\mathbf{x}, t; \theta); \quad \Pi = \Pi(\mathbf{x}, t; \theta).$$

(20)

4.2 Chaos Expansion. We apply the generalized polynomial chaos expansion, or the Askey-chaos (2), to these quantities and obtain

$$\mathbf{u}(\mathbf{x}, t; \theta) = \sum_{i=0}^{P} \mathbf{u}_i(\mathbf{x}, t) \Phi_i(\boldsymbol{\xi}(\theta));$$

$$\Pi(\mathbf{x}, t; \theta) = \sum_{i=0}^{P} \Pi_i(\mathbf{x}, t) \Phi_i(\boldsymbol{\xi}(\theta)).$$

(21)

Substituting (21) into Navier-Stokes equations we obtain the following equations

$$\sum_{i=0}^{P} \nabla \cdot \mathbf{u}_i(\mathbf{x}, t) \Phi_i = 0,$$

(22)

$$\sum_{i=0}^{P} \frac{\partial \mathbf{u}_i(\mathbf{x}, t)}{\partial t} \Phi_i + \sum_{i=0}^{P} \sum_{j=0}^{P} [(\mathbf{u}_i \cdot \nabla) \mathbf{u}_j)] \Phi_i \Phi_j$$

$$= -\sum_{i=0}^{P} \nabla \Pi_i(\mathbf{x}, t) \Phi_i + \mathrm{Re}^{-1} \sum_{i=0}^{P} \nabla^2 \mathbf{u}_i \Phi_i.$$

(23)

We then project the above equations onto the random space spanned by the basis polynomials $\{\Phi_i\}$ by taking the inner product of above equation with each basis. By taking $\langle \cdot, \Phi_k \rangle$ and utilizing the orthogonality condition (3), we obtain the following set of equations:

For each $k = 0, \ldots P$,

$$\nabla \cdot \mathbf{u}_k = 0,$$

(24)

$$\frac{\partial \mathbf{u}_k}{\partial t} + \frac{1}{\langle \Phi_k^2 \rangle} \sum_{i=0}^{P} \sum_{j=0}^{P} e_{ijk} [(\mathbf{u}_i \cdot \nabla) \mathbf{u}_j)] = -\nabla \Pi_k + \mathrm{Re}^{-1} \nabla^2 \mathbf{u}_k,$$

(25)

where $e_{ijk} = \langle \Phi_i \Phi_j \Phi_k \rangle$. The set of equations consists of $(P+1)$ system of deterministic 'Navier-Stokes-like' equations for each random mode coupled through the convective terms.

4.3 Numerical Discretization. Discretization in space and time can be carried out by any conventional method. Here we

employ the spectral/hp element method in space in order to have better control of the numerical error [29]. The high-order splitting scheme together with properly defined consistent pressure boundary conditions are employed in time [30]. In particular, the spatial discretization is based on Jacobi polynomials on triangles or quadrilaterals in two-dimensions, and tetrahedra, hexahedra or prisms in three-dimensions.

4.4 Post-Processing. After solving the *deterministic* expansion coefficients, we obtain the analytical form (in random space) of the solution process. It is possible to perform a number of analytical operations on the stochastic solution in order to carry out other analysis such as the sensitivity analysis. The *mean* solution is contained in the expansion term with index of zero. The *second-moment*, i.e., the *covariance function* is given by

$$R_{\mathbf{uu}}(\mathbf{x}_1,t_1;\mathbf{x}_2,t_2) = \langle \mathbf{u}(\mathbf{x}_1,t_1) - \overline{\mathbf{u}(\mathbf{x}_1,t_1)}, \mathbf{u}(\mathbf{x}_2,t_2) - \overline{\mathbf{u}(\mathbf{x}_2,t_2)} \rangle$$

$$= \sum_{i=1}^{P} [\mathbf{u}_i(\mathbf{x}_1,t_1)\mathbf{u}_i(\mathbf{x}_2,t_2)\langle \Phi_i^2 \rangle]. \qquad (26)$$

Note that the summation starts from index ($i=1$) instead of 0 to exclude the mean, and that the orthogonality of the Askey-chaos basis $\{\Phi_i\}$ has been used in deriving the above equation. Similar expressions can be obtained for the pressure field.

Implementation details and verifications of the stochastic Navier-Stokes solver can be found in [16].

5 Flow-Structure Interactions

In this section we consider two-dimensional vortex-induced vibrations of an elastically-mounted circular cylinder subject to stochastic inputs. The computational domain is shown in Fig. 3 where the circular cylinder with unit diameter ($D=1$) is located at the origin. The size of the domain is $[-15,25]\times[-9,9]$. There are 412 triangular elements and sixth-order Jacobi polynomials in each element are found to be sufficient to resolve the flow in the physical space in the range of Re$<$200. The Reynolds number is defined as Re$=U_\infty D/\nu$, where U_∞ is the inflow and ν the kinematic viscosity.

5.1 Structure Problem. In this paper we will focus on the cross-flow displacement of the cylinder, i.e., the cylinder is free to move in the y-direction but not in the x-direction. For a linear structure, the governing equation is the second-order ordinary differential equation

$$\rho \frac{d^2\eta}{dt^2} + b\frac{d\eta}{dt} + K\eta = F(t), \qquad (27)$$

where ρ, b and K are the mass, damping and stiffness of the cylinder, and the natural frequency of this system is $\omega_n = \sqrt{K/\rho}$. For clarity, we rewrite Eq. (27) in the same form as in (11):

$$\frac{d^2\eta}{dt^2} + c\frac{d\eta}{dt} + k\eta = f(t), \qquad (28)$$

where $c=b/\rho$, $k=K/\rho$ and $f(t)=F(t)/\rho$. The external force $f(t)$ comes from the flow and we incorporate uncertain components in c and k in the following simulations.

5.2 Transformed Navier-Stokes Equations. To couple the flow with moving boundaries of the structure, one can employ Arbitrary Lagrangian-Eulerian (ALE) method. Although general, this approach is computationally expensive so we consider a boundary-fitted coordinate approach for the specific problem we solve here. By attaching the coordinate system to the cylinder, the cylinder appears stationary in time (with respect to that coordinate system). Following [31], we define two coordinate systems: (x',y',t') and (x,y,t), where (x',y',t') is the original coordinate system and (x,y,t) is the transformed one. The mapping between the two systems is

$$x=x',$$

$$y=y'-\eta(t'),$$

$$t=t'.$$

In two-dimensional flow, this simply reduces to the v velocities being shifted by the reference frame velocity,

$$u=u',$$

$$v=v'-\frac{d\eta}{dt'},$$

$$p=p'.$$

It is worth noting that this mapping is stochastic when the cylinder motion is random and needs to be represented by the chaos expansion as well.

The incompressible Navier-Stokes equations are transformed into:

$$\nabla \cdot \mathbf{u}=0, \qquad (29)$$

$$\frac{\partial \mathbf{u}}{\partial t} + (\mathbf{u}\cdot\nabla)\mathbf{u} = -\nabla\Pi + \mathrm{Re}^{-1}\nabla^2\mathbf{u} + \mathbf{A}(t), \qquad (30)$$

where $A_x=0$ and $A_y=-d^2\eta/dt^2$.

In the following simulations, we assume the damping c and stiffness k in Eq. (28) to be random variables. Then the structure response becomes a random process, so does the psuedoforcing $\mathbf{A}(\mathbf{t})$ in the transformed Navier-Stokes equations. This, in turn, makes the flow field random, which exerts a stochastic dynamic forcing $f(t)$ back onto the cylinder. The entire coupled system
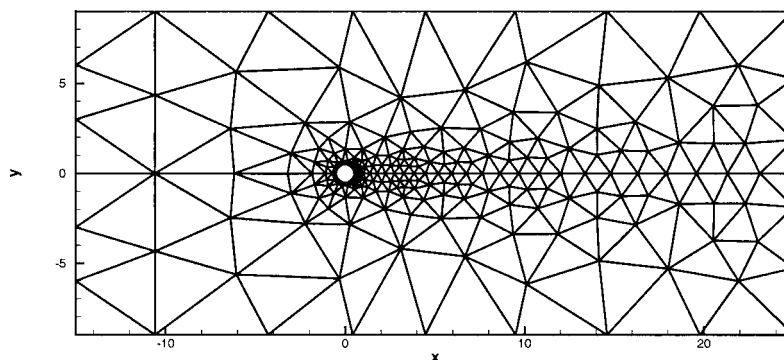

Fig. 3 Schematic of the domain for flow past an elastically mounted circular cylinder
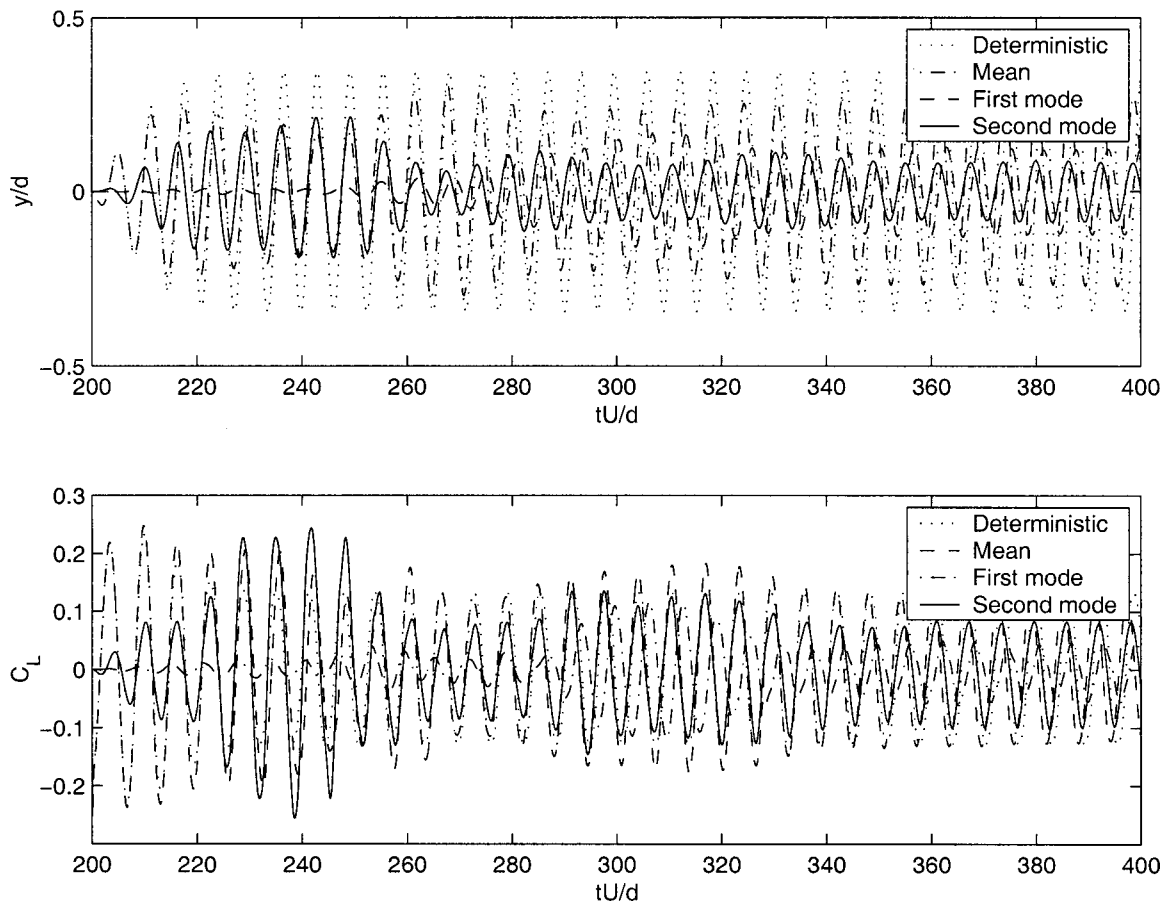
Fig. 4 Dominant random modes of the cylinder motion. Upper: modes of the cross-flow displacement *y/D*; lower: modes of the lift coefficient *C_L*.

then becomes stochastic. The same expansion procedure as in Section 4 is employed, with the psuedo-forcing $\mathbf{A}(t)$ and the mapping expanded appropriately, too.

5.3 Numerical Results. We assume that the Reynolds number is fixed at Re=100, and we also assume that the input parameters of the cylinder are uncertain, i.e., $c=\bar{c}+\sigma_c\xi_1$ and $k=\bar{k}+\sigma_k\xi_2$, where ξ_1 and ξ_2 are two independent standard Gaussian random variables with zero mean and unit variance. The mean and standard deviation of c and k are set as $(\bar{c},\sigma_c)=(0.1,0.01)$ and $(\bar{k},\sigma_k)=(1.0,0.2)$, respectively. We choose $\bar{k}=1.0$ such that the natural frequency of the oscillator is close to the frequency of the vortex shedding of the fixed cylinder at Re=100, and the cylinder response is maximized. According to the uncertain inputs, we employ the two-dimensional ($n=2$) Hermite-chaos, the corresponding Askey-chaos for Gaussian inputs as shown in Table 1, as the trial basis in random space. A third-order Hermite-chaos ($p=3$) is employed which results in a 10-term chaos expansion ($P=9$ according to Eq. (16)). Therefore, the computational cost (serial) of this run is about 10 times more than the cost of the corresponding deterministic simulation. In particular, the cost of the structure solver, even if it is nonlinear, is negligible compared to the flow solver. The fluid forces on the cylinder are computed using

$$\mathbf{F}=\oint[-\mathbf{n}\Pi+\text{Re}^{-1}(\nabla\mathbf{u}+\nabla\mathbf{u}^T)\cdot\mathbf{n}]ds,$$

where $\mathbf{n}$ is the outward normal on the cylinder and ds is the arc length on the surface of the cylinder. The corresponding force coefficients are computed by nondimensionalizing the forces with the fluid density ρ_f, free-stream velocity U_∞ and the cylinder diameter D:

$$C_D=\frac{F_D}{\frac{1}{2}\rho_f DU_\infty^2},\quad C_L=\frac{F_L}{\frac{1}{2}\rho_f DU_\infty^2}.$$

In Fig. 4 we plot the time evolution of the first few coefficients of the dominant random modes of the nondimensional cross-flow displacement (y/D) and the lift coefficient (C_L), together with the deterministic solution. We see that due to the effective diffusion of the randomness, the mean response of y/D has smaller amplitude compared to its deterministic counterpart. The first and second random modes, as shown in the figure, correspond to the Gaussian part of the response.

In Fig. 5 we show the time evolution of the variances of the cross-flow displacement y/D and lift coefficient C_L. We see that the variance peaks at the early transition stage before it settles to the asymptotic periodic state. The peak value is 2–3 times larger than that of the final periodic state. This suggests that the system responses to the uncertain inputs are important in the early transition stage and also non-negligible in the final asymptotic state.

Figure 6 shows the instantaneous contours of the rms of the vorticity field at $t=600$ (nondimensional time units) corresponding to more than 100 shedding cycles. The center location of the cylinder is not at the origin as shown in the figure. It is interesting that the regions with the largest uncertainty are regions of the most importance from the fluid dynamical point of view, i.e., the shear layer and near-wake but not the far-field.

In Fig. 7 the instantaneous pressure distribution along the surface of the cylinder at $t=600$ is shown. Here θ is the angle of the location on the surface with $\theta=0$ the rear stagnation point and $\theta=\pi$ the front stagnation point. The error-bar curve is centered at the mean of the stochastic pressure solution and the length of the
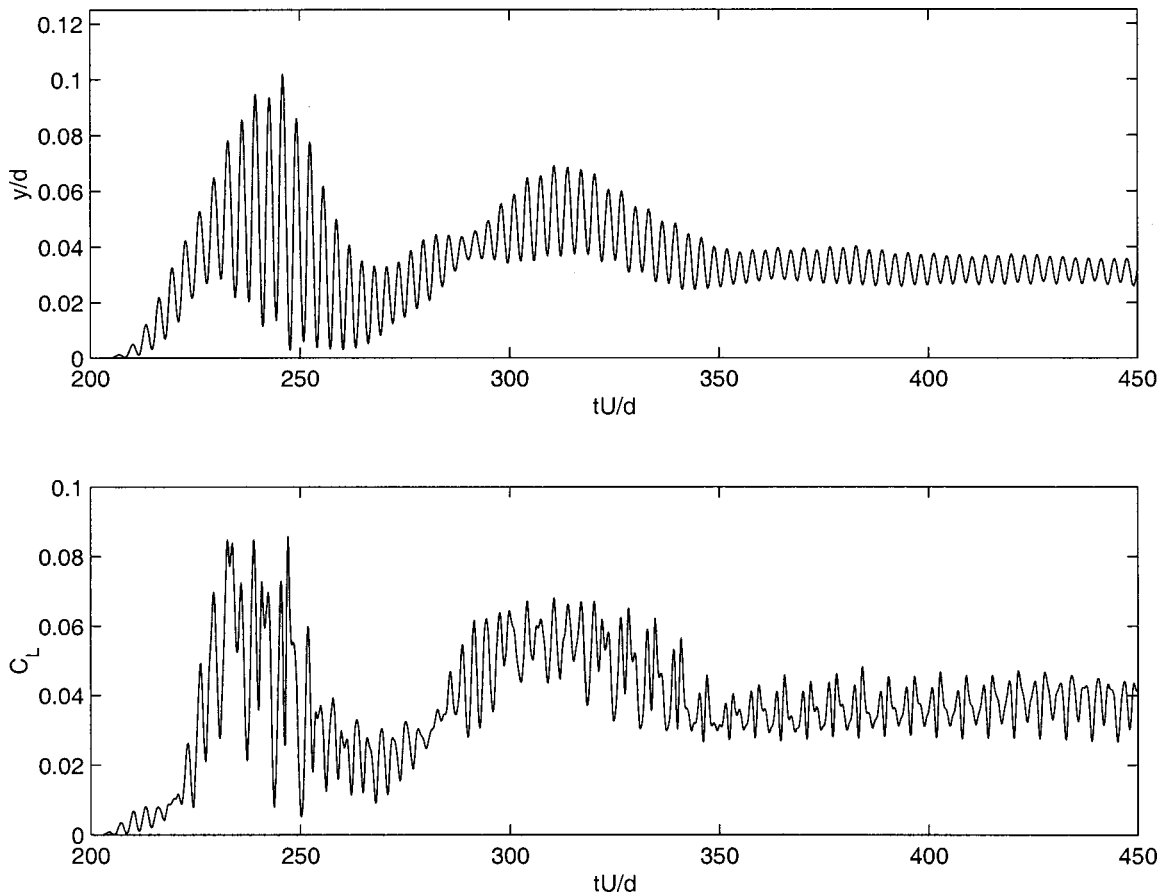
Fig. 5 Variance of the cylinder motion. Upper: variance of the cross-flow displacement y/D, lower, variance of the lift coefficient C_L.
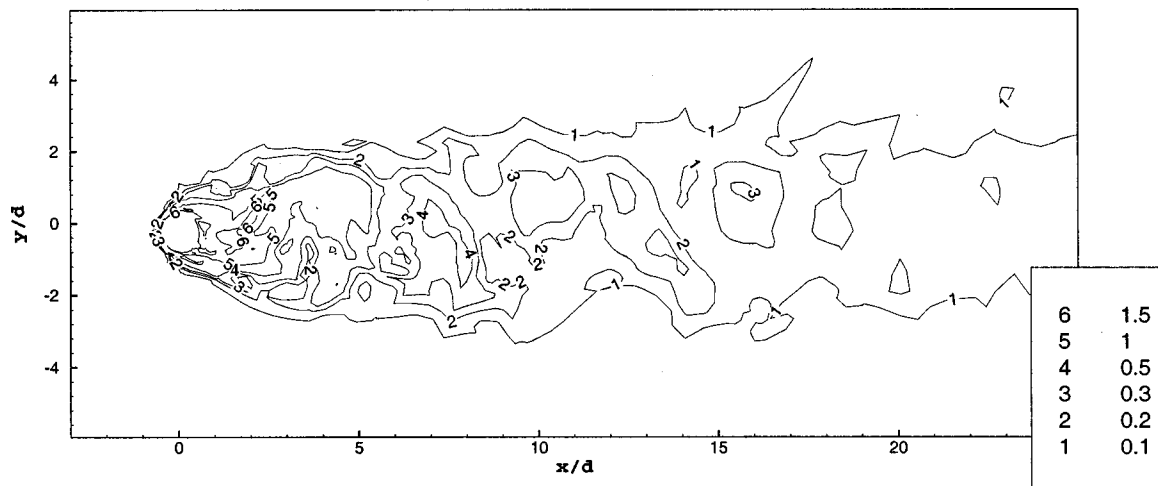

Fig. 6 Regions of uncertainty: instantaneous *rms* of vorticity

bars indicates two standard deviations around the mean (i.e., one above and one below the mean). For comparison, the deterministic pressure distribution at the same instance is shown as well. The difference compared with stochastic mean solution is noticeable; for the chosen magnitudes of variance of the stochastic inputs, the deterministic signal remains inside the "envelope" of the stochastic solution at this instance.

6 Summary and Discussion

We have developed a stochastic spectral method to model uncertainty and its propagation in flow simulations. More specifi-

cally, we have generalized the original polynomial chaos idea of Wiener and proposed a broader framework, i.e., the Askey-chaos, which includes Wiener's Hermite-chaos as a subset. Numerical examples were presented for relatively simple systems, such as a second-order ordinary differential equation and a more complicated flow-structure interaction problem at relatively low Reynolds number. We do not yet have experience with such stochastic simulations at high Reynolds number.

The method we developed here is general and can also be applied to model uncertainty in the boundary domain, e.g., a rough
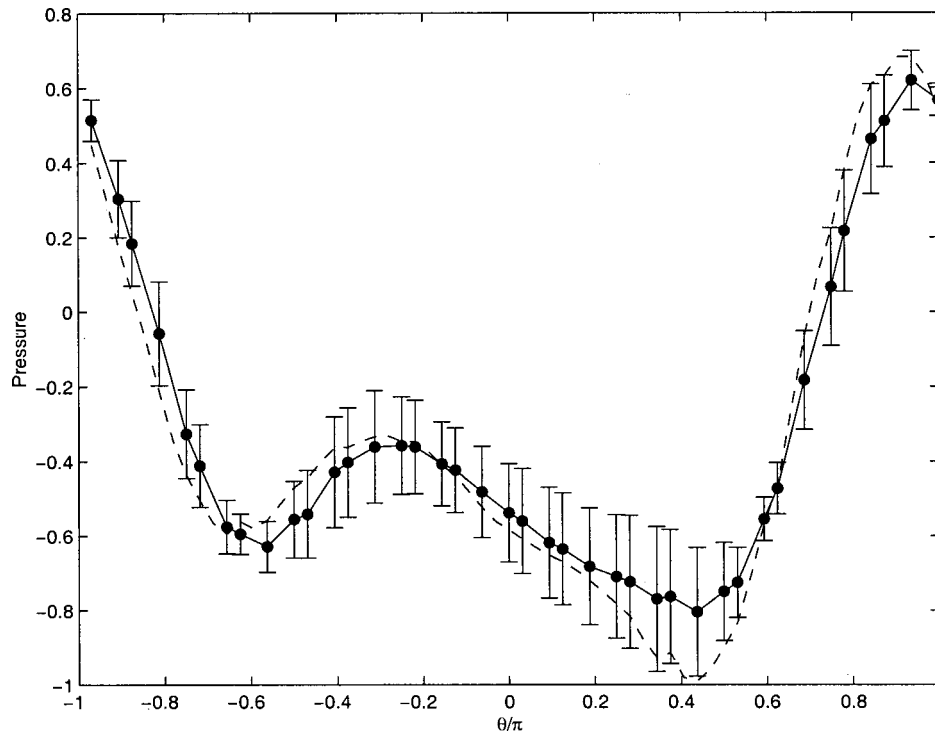
Fig. 7 Instantaneous pressure distribution along the surface of the cylinder; error-bar: stochastic solution, dashed line: deterministic solution

surface, in the transport coefficients, e.g., the eddy viscosity in large eddy simulations, and other problems. It provides a formal procedure for constructing a *composite error bar* for CFD applications, as proposed in [32], that includes, in addition to the discretization errors, contributions due to imprecise physical inputs to the simulations.

As regards efficiency, a single Askey-chaos based simulation, albeit computationally more expensive than the corresponding deterministic solver, is able to generate the solution statistics in a single run. In contrast, for the Monte Carlo simulation, tens of thousands of realizations are required for converged statistics, which is prohibitively expensive for most CFD problems in practice. Further work will include simulations with different distribution functions and their corresponding Askey-chaos expansion as presented here.

Acknowledgments

References

[1] Ziada, S. and Staubli, T., (editors), 2000, "Flow-Induced Vibration," Proc. 7th Int. Conf., FIV2000, Lucerne, Switzerland, 19–22 June, A. A. Balkema.

[2] Leweke, T. (editor), 2001, "Special Issue on Proc. of IUTAM Symposium on Bluff Body Wakes and Vortex-Induced Vibrations, Marseille, France, 13–16 June 2000," J. Fluids Struct. .

[3] Shlesinger, M. F. and Swean, T., 1998, *Stochastically Excited Nonlinear Ocean Structures*, World Scientific.

[4] Hills, R. G., and Trucano, T. G., 1999, "Statistical Validation of Engineering and Scientific Models: Background," Technical Report SAND99-1256, Sandia National Laboratories.

[5] Shinozuka, M., and Deodatis, G., 1986, "Response Variability of Stochastic Finite Element Systems," Technical Report, Dept. of Civil Engineering, Columbia University, New York.

[6] Ghanem, R. G., and Spanos, P., 1991, *Stochastic Finite Elements: A Spectral Approach*, Springer-Verlag.

[7] Wiener, N., 1938, "The Homogeneous Chaos," Am. J. Math., **60**, pp. 897–936.

[8] Wiener, N., 1958, *Nonlinear Problems in Random Theory*, MIT Technology Press Wiley, New York.

[9] Meecham, W. C., and Siegel, A., 1964, "Wiener-Hermite Expansion in Model Turbulence at Large Reynolds Numbers," Phys. Fluids, **7**, pp. 1178–1190.

[10] Siegel, A., Imamura, T., and Meecham, W. C., 1965, "Wiener-Hermite Expansion in Model Turbulence in the Late Decay Stage," J. Math. Phys., **6**, pp. 707–721.

[11] Meecham, W. C., and Jeng, D. T., 1968, "Use of the Wiener-Hermite Expansion for Nearly Normal Turbulence," J. Fluid Mech., **32**, pp. 225–249.

[12] Orszag, S. A., and Bissonnette, L. R., 1967, "Dynamical Properties of Truncated Wiener-Hermite Expansions," Phys. Fluids, **10**, p. 2603.

[13] Crow, S. C., and Canavan, G. H., 1970, "Relationship Between a Wiener-Hermite Expansion and an Energy Cascade," J. Fluid Mech., **41**, pp. 387–403.

[14] Chorin, A. J., 1974, "Gaussian Fields and Random Flow," J. Fluid Mech., **85**, pp. 325–347.

[15] Xiu, D., and Karniadakis, G. E., 2001, "The Wiener-Askey Polynomial Chaos for Stochastic Differential Equations," SIAM J. Sci. Comput. (USA), submitted.

[16] Xiu, D., and Karniadakis, G. E., 2001, "Modeling Uncertainty in Flow Simulations Via Generalized Polynomial Chaos," J. Comput. Phys., to appear.

[17] Askey, R., and Wilson, J., 1985, "Some Basic Hypergeometric Polynomials that Generalize Jacobi Polynomials," Memoirs Amer. Math. Soc., AMS, Providence RI, **54**, No. 319, pp. 1–55.

[18] Hou, Z., Zhou, Y., Dimentberg, M. F., and Noori, M., 1996, "A Stationary Model for Periodic Excitation with Uncorrelated Random Disturbances," Probab. Eng. Mech., **11**, pp. 191–203.

[19] Yim, S. C. S., and Lin, H., 1998, "A Methodology for Analysis and Design of Sensitive Nonlinear Ocean Systems, *Stochastically Excited Nonlinear Ocean Structures*, World Scientific, p. 105.

[20] Soong, T. T., and Grigoriu, M., 1993, *Random Vibration of Mechanical and Structural Systems*, Prentice Hall.

[21] Fei, C.-Y., and Vandiver, J. K., 1995, "A Gaussian Model for Predicting the Effect of Unsteady Windspeed on the Vortex-Induced Vibration Response of Structural Members," J. Struct. Mech., ASME, Proc. 14th Int. Conf. on Offshore Mechanics and Arctic Engineering, Book No. H00939:57–65.

[22] Shinozuka, M., Yun, C., and Vaicatis, R., 1977, "Dynamic Analysis of Fixed Offshore Structures Subject to Wind Generated Waves," J. Struct. Mech., **5**, No. 2, pp. 135–146.

[23] Grigoriu, M., 1984, "Extremes of Wave Forces," J. Eng. Mech., **110**, pp. EM12:1731–1742.

[24] Schoutens, W., 2000, *Stochastic Processes and Orthogonal Polynomials*, Springer-Verlag New York.

[25] Koekoek, R., and Swarttouw, R. F., 1998, "The Askey-Scheme of Hypergeometric Orthogonal Polynomials and its Q-Analogue," Technical Report 98-17, Department of Technical Mathematics and Informatics, Delft University of Technology.

[26] Cameron, R. H., and Martin, W. T., 1997, "The Orthogonal Development of Nonlinear Functionals in Series of Fourier-Hermite Functionals," Ann. Math., **48**, p. 385.

[27] Ogura, H., 1972, "Orthogonal Functionals of the Poisson Process," IEEE Trans. Inf. Theory, **IT-18**, pp. 473–481.

[28] Loève, M., 1977, *Probability Theory, Fourth edition*, Springer-Verlag.

[29] Karniadakis, G. E., and Sherwin, S. J., 1999, *Spectral/hp Element Methods for CFD*, Oxford University Press.

[30] Karniadakis, G. E., Israeli, M., and Orszag, S. A., 1991, "High-Order Splitting Methods for Incompressible Navier-Stokes Equations," J. Comput. Phys., **97**, p. 414.

[31] Newman, D. J., and Karniadakis, G. E., 1997, "Simulations of Flow Past a Freely Vibrating Cable," J. Fluid Mech., **344**, pp. 95–136.

[32] Karniadakis, G. E., 1995, "Towards an Error Bar in CFD," ASME J. Fluids Eng., **117**, pp. 7–9.